Statistical downscaling of historical monthly mean winds over a coastal region of complex terrain. I. Predicting wind speed

Charles L. Curry, D. W. van der Kamp, & Adam H. Monahan

2012

Original citation:

Curry, C. L., van der Kamp, D. W., & Monahan, A. H. (2012). Statistical downscaling of historical monthly mean winds over a coastal region of complex terrain. I. Predicting wind speed. Climate Dynamics, 38(7–8), 1281–1299. https://doi.org/10.1007/s00382-011-1173-3

Clim Dyn (2012) 38:1281–1299
DOI 10.1007/s00382-011-1173-3

Statistical downscaling of historical monthly mean winds over a coastal region of complex terrain. I. Predicting wind speed

Charles L. Curry · Derek van der Kamp · Adam H. Monahan

Received: 14 October 2010 / Accepted: 17 August 2011 / Published online: 17 September 2011

Abstract Surface wind speed is a key climatic variable of interest in many applications, including assessments of storm-related infrastructure damage and feasibility studies of wind power generation. In this work and a companion paper (van der Kamp et al. 2011), the relationship between local surface wind and large-scale climate variables was studied using multiple regression analysis. The analysis was performed using monthly mean station data from British Columbia, Canada and large-scale climate variables (predictors) from the NCEP-2 reanalysis over the period 1979–2006. Two regression-based methodologies were compared. The first relates the annual cycle of station wind speed to that of the large-scale predictors at the closest grid box to the station. It is shown that the relatively high correlation coefficients obtained with this method are attributable to the dominant influence of region-wide seasonality, and thus contain minimal information about local wind behaviour at the stations. The second method uses interannually varying data for individual months, aggregated into seasons, and is demonstrated to contain intrinsically local information about the surface winds. The dependence of local wind speed upon large-scale predictors over a much larger region surrounding the station was also explored, resulting in 2D maps of spatial correlations. The cross-validated explained variance using the interannual method was highest in autumn and winter, ranging from 30 to 70% at about a dozen stations in the region. Reasons for the limited predictive skill of the regressions and directions for future progress are reviewed.

Keywords Wind · Statistical downscaling · Regional climate · North America

C. L. Curry (✉)
Canadian Centre for Climate Modelling and Analysis,
Environment Canada, University of Victoria,
Victoria, BC V8W 3V6, Canada
e-mail: cc@uvic.ca

C. L. Curry · D. van der Kamp · A. H. Monahan
School of Earth and Ocean Sciences, University of Victoria,
Victoria, BC V8W 3V6, Canada

D. van der Kamp
Pacific Climate Impacts Consortium, University of Victoria,
Victoria, BC V8W 2Y2, Canada

1 Introduction

There is increasing demand for high resolution, or site-specific, information from climate models that simulate future climate change. This need is motivated by the recognition that global scale, low frequency climate forcings (e.g., due to increasing greenhouse gases and aerosols) drive changes in coupled atmosphere–ocean behaviour at scales of hundreds to thousands of km that, in turn, are manifested as local, high-frequency impacts on much smaller scales ($\sim$1 km or less; Giorgi et al. 2001). On the largest scales, coupled global climate models (GCMs) are used to solve the relevant meteorological equations of motion. Subsequently, information from a GCM can be used as boundary conditions for a nested simulation of climate at a resolution of tens of km, centred on a particular region of interest. The "dynamical downscaling" provided by these regional climate models (RCMs) has provided detailed information for many regions worldwide (Music and Caya 2007; Wang et al. 2009; Marengo et al. 2010). Nevertheless, for those interested in climate indicators at the kilometre scale or less, some form of further downscaling of model results is required.

Many techniques of interpolation or statistical downscaling have been applied with this objective in mind. The

utility and merits of each depends on the variable being downscaled and the specific application. A majority of the downscaling methods that have appeared in the literature are based on simple linear regression using either observational data or GCM/RCM output as predictands, although other techniques are increasingly applied, including nonlinear regression, weather classification, and stochastic weather generators (for a review of various methods see Giorgi et al. 2001). While most attention to date has focused on surface temperature and precipitation (see Wilby et al. 1998 and Giorgi et al. 2001 for comprehensive reviews), the statistical downscaling of surface wind speeds, the focus of this paper, is a relatively recent development (Troen and Peterson 1989; Sailor et al. 2000, 2008; de Rooy and Kok 2004; Pryor et al. 2005, 2006; Michelangeli et al. 2009; Salameh et al. 2009). One should keep in mind that downscaling methods used with some success for surface temperature and precipitation may not be as effective when applied to wind, for a number of reasons. Chief among these are the intermittency of wind and its vector character, as well as its sensitivity to local topographic features and surface roughness. The recent work of Salameh et al. (2009) on wind downscaling in the French Alps provides an instructive example of how steep topography, in particular, can strongly constrain an effective downscaling methodology.

Wigley et al. (1990) attempted to evaluate the effectiveness of conventional linear regression for downscaling by regressing temperature and precipitation measurements at individual meteorological stations in Oregon against regional averages of the same quantities, along with mean sea-level pressure, its horizontal gradient, and (as an alternate set of predictors) the same fields at 700 hPa height. Our approach is similar in spirit, in that we are interested in establishing relations between two sets of observations, large- and small-scale, and then evaluating the predictive power of such relations at the various stations. Specifically, we represent the local surface wind speed measurements over each month as a two-parameter Weibull distribution, and use monthly mean NCEP-2 reanalysis fields as the large-scale predictors. If the downscaling relations so derived are not robust, then the use of the same approach in the context of future climate model projections will need to be reconsidered. We show that, in the region considered in this paper, there are serious concerns with at least one approach and evident limitations in other regression-based methods that use surface wind speed as a predictand. In a companion paper (van der Kamp et al. 2011, hereafter Paper II), alternative predictands of surface wind are explored, specifically the use of individual wind components.

While the particular region studied here, British Columbia on Canada's west coast (hereafter BC), has not been the focus of any wind downscaling studies to date, related work has been published recently. Selected stations in BC were included in the downscaling studies of Sloughter et al. (2010) and Thorarinsdottir and Gneiting (2010), which focused on short-range forecasting of wind speed over the Pacific Northwest. Extreme wind recurrence frequency at three stations in southern BC was analyzed in the context of larger-scale climate variability by Abeysirigunawardena et al. (2009). Wind speed trends in recent decades at selected meteorological stations in the region were examined by Tuller (2004), while the behaviour of past and future GCM-modelled marine winds off BC was addressed by Merryfield et al. (2009). Accessible characterizations of the overall weather and climate of the Pacific Northwest region including winds may be found in Lange (2003) and Mass (2008). Finally, we note that while the limitations of downscaling methods mentioned in the previous paragraph were encountered on this specific domain, there is reason to believe they may manifest themselves in many other regions as well.

2 Observational data and downscaling methodology

2.1 Station and reanalysis data

Long-term measurements of hourly near-surface (10 m height) wind speed at 20 WMO-certified stations within the study domain were obtained from Environment Canada's Climate Data Online website, http://climate.weatheroffice.gc.ca/climateData/canada_e.html. The raw time series from these 20 stations were corrected for non-standard anemometer height and spurious trends by Wan et al. (2010), resulting in a 28-year (1979–2006), homogenized, monthly time series of wind speed and its standard deviation. Geographic locations and other details are displayed in Fig. 1; Table 1 (these data are available via the Canadian Centre for Climate Modelling and Analysis website, http://www.cccma.ec.gc.ca/hccd/index_e.shtml). Monthly mean large-scale data, used as predictors (Sect. 3), were taken from the NCEP/DOE AMIP-II reanalysis (R-2) for the same time period (Kanamitsu et al. 2002).

2.2 Characterizing the observed surface wind speed distribution

The temporal behaviour of the surface wind speed $W(t)$ at any location may be represented by a histogram of occurrence frequency versus W. Previous research has demonstrated that the two-parameter Weibull distribution provides a useful analytic approximation to the observed histogram under a broad range of circumstances (Justus et al. 1978; Conradsen, Nielsen, and Prahm 1984; Monahan

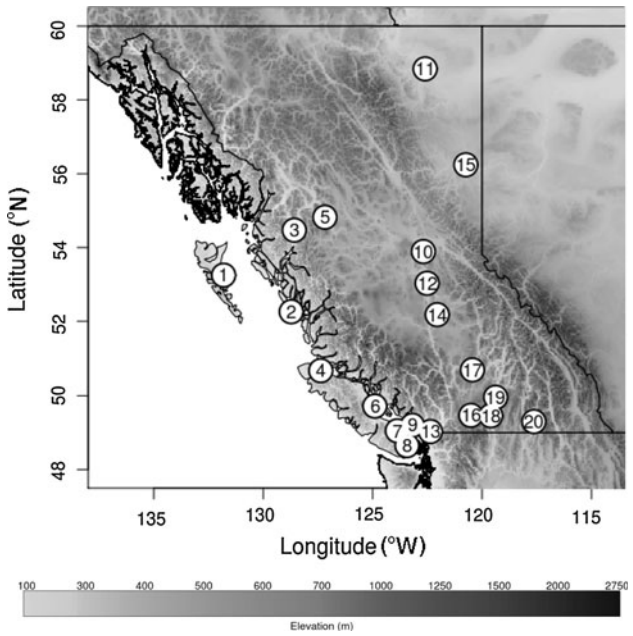

Fig. 1 Meteorological stations used in this study. See Table 1 for further details

Table 1 Meteorological stations used in this study

ID	Station name	Latitude (°N)	Longitude (°W)	Elevation (m)
1	Sandspit A	53.25	131.81	6
2	McInnes Island	52.26	128.72	26
3	Terrace A	54.47	128.58	217
4	Port Hardy A	50.68	127.37	22
5	Smithers A	54.82	127.18	522
6	Comox A	49.72	124.90	26
7	Nanaimo A	49.05	123.87	28
8	Victoria Int'l A	48.65	123.43	19
9	Vancouver Int'l A	49.20	123.18	4
10	Prince George A	53.89	122.68	691
11	Fort Nelson A	58.84	122.60	382
12	Quesnel A	53.03	122.51	545
13	Abbotsford A	49.03	122.36	59
14	Williams Lake A	52.18	122.05	940
15	Fort St. John A	56.24	120.74	695
16	Princeton A	49.47	120.51	700
17	Kamloops A	50.70	120.44	345
18	Penticton A	49.46	119.60	344
19	Kelowna A	49.96	119.38	430
20	Castlegar A	49.30	117.63	495

All stations are located at airports, with the exception of McInnes Island, and are WMO certified. Original data are at hourly resolution but many stations have occasional gaps. All stations are in the adjusted homogenized data set of Wan et al. (2010), which is at monthly resolution, continuous over the period 1979/01–2006/12, with the exception of Sandspit (1979/01–2004/12) and McInnis Island (1979/01–2001/11)

2006 and references therein; He et al. 2010). The Weibull probability density function (PDF) is

$$p(W) = \frac{k}{A}\left(\frac{W}{A}\right)^{k-1} \exp\left[-\left(\frac{W}{A}\right)^{k}\right]$$

where $W \geq 0$ is the wind speed (m s^{-1}), $A > 0$ (m s^{-1}) is a scale parameter closely related to the mean of the distribution, and $k > 0$ is a dimensionless shape parameter. In some cases, the addition of a third parameter that effectively shifts the distribution along the W-axis has been shown to provide improved fits to data (Stewart and Essenwanger 1978; van der Auwera et al. 1980; Tuller and Brett 1985), but we neglect this refinement here. The mean and standard deviation of the Weibull distribution are given by

$$\bar{W} = A\Gamma\left(1+\frac{1}{k}\right),$$

$$\sigma_W = A\left[\Gamma\left(1+\frac{2}{k}\right) - \Gamma^2\left(1+\frac{1}{k}\right)\right]^{1/2},$$

where $\Gamma(x)$ is the gamma function. The above equations may be inverted to give A and a good approximation to k in terms of $\bar{W}$ and σ_W (Justus et al. 1978):

$$A = \frac{\bar{W}}{\Gamma\left(1+\frac{1}{k}\right)}, \quad k \approx \left[\frac{\bar{W}}{\sigma_W}\right]^{1.086}.$$

In the relevant range of $k > 1$, A differs from $\bar{W}$ by at most 13%. By contrast, k is equally sensitive to both $\bar{W}$ and σ_W. The Weibull PDF reduces to the exponential distribution when $k = 1$, the Rayleigh distribution when $k = 2$, and is nearly Gaussian for $k = 3.6$. Over land in the mid-latitudes, the histogram of observed winds is generally positively skewed, meaning that the best-fit $k < 3.6$ (He et al. 2010). The parameters A and k are used to characterize the observed wind distributions used in this study. In particular, they function as predictands (dependent variables) in the downscaling method described in the following section.

Examples of piecewise integrated Weibull PDF fits to histograms of the raw, hourly wind speeds at several stations are shown in Fig. 2. Two of the stations (Vancouver and McInnes Island) are representative of coastal locations, while the other two are in the BC interior. Three of the stations have very similar PDFs, as reflected by their fitted A (7.8 to 8.6 m s^{-1}) and k (1.7–1.8) values, but McInnes Island is significantly different ($A = 18.7$ m s^{-1}, $k = 1.6$). While both McInnes Island and Vancouver are coastal, the former is much more exposed to strong westerly storm fronts of the Northeast Pacific, thus accounting for its significantly larger mean wind speed (i.e., A value). We also computed A and k using once-daily (1300 local time) sampling from the original, unadjusted data, but found this did not strongly affect the fitted parameters once they were

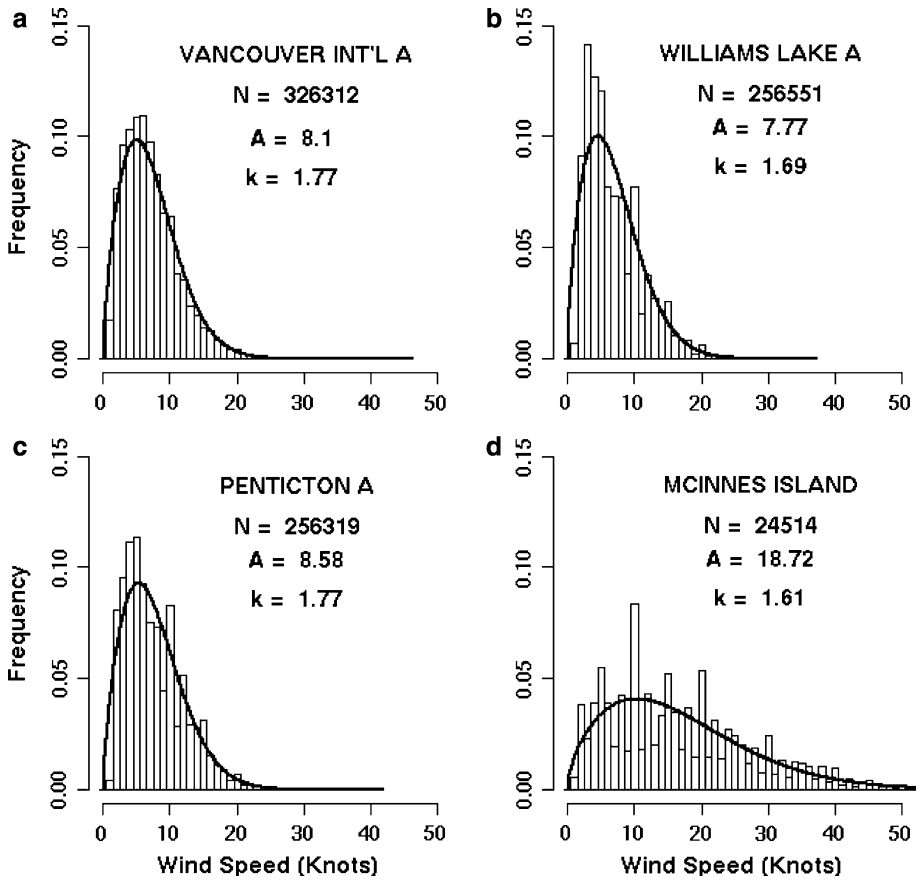

Fig. 2 Piecewise-integrated Weibull PDF fits to histograms of hourly wind speeds over the entire 1979–2006 period at four stations: a Vancouver; b Williams Lake; c Penticton; and d McInnes Island. Histograms are normalized to the total number of observations at each site, given below the station label. Weibull parameters derived from the fits are also given on each panel

monthly averaged. Hence, we use the homogenized data throughout this analysis except where otherwise noted.

2.3 Empirical downscaling method

For the purpose of this study, we assume that some form of empirical downscaling is appropriate, wherein a transfer function is sought that statistically relates some locally measured near-surface field of interest (here, wind speed, as characterized by the Weibull PDF) to larger scale fields; the latter might be derived from reanalysis observations (here, NCEP-2), or alternatively, from a GCM/RCM. The transfer function at a particular observational station is represented by multiple linear regression relations of the form (e.g., Wigley et al. 1990; Pryor et al. 2005)

$$\begin{aligned} \overline{A}_{1,\ldots,n} &= a_0 + \sum_{j=1}^{N_A} a_j \overline{P}_{1,\ldots,n,j} + \varepsilon_A, \\ \overline{k}_{1,\ldots,n} &= b_0 + \sum_{j=1}^{N_k} b_j \overline{Q}_{1,\ldots,n,j} + \varepsilon_k, \end{aligned} \tag{1}$$

where the index n denotes the number of data points entering the regression, the overbar denotes a suitable time mean (e.g., monthly), sums are over $j = 1, \ldots, N_A$ large-scale predictors P_j for A, N_k predictors Q_j for k, and ε_A and ε_k are residuals of the fit. The predictor values usually correspond to the closest large-scale grid point to the station of interest; in some cases bi-linear interpolation or gradients between neighbouring points may be more appropriate. If large-scale telecommunication patterns are thought to be important, P_j and Q_j might involve contributions from locations more distant from the station; an example of this approach will be presented in Sect. 4. The choice of predictors to characterize the wind fields is highly subjective, varies widely, and is often based largely on heuristic considerations. Several types of predictors and the means for choosing between them will be examined in the following analysis.

3 Local downscaling of surface wind variations

In this section, two different methods of calibrating the regression relation (1) are examined and applied to the BC region. Both use local (i.e., closest grid point) values of the same large-scale predictors, although we incorporate additional/alternate predictors in Sect. 3.2. We shall see that the type of information contained in the regression coefficients determined by each technique differs, and that this affects the interpretation and scope of applicability of each.

3.1 Use of the seasonal cycle and associated caveats

One method of calibrating Eq. (1) that has been employed in the context of both surface temperature and wind downscaling is to make use of seasonal variations in these quantities (Sailor and Li 1999; Sailor et al. 2000, 2008; Pryor et al. 2005, hereafter PSB05; Pryor et al. 2006). In the method of PSB05, applied over northern Europe/Scandinavia, the transfer function (1) at each station is expressed as

$$\overline{\overline{A}}_m = a_0 + \sum_{j=1}^{N_A} a_j \overline{\overline{P}}_{j,m} + \varepsilon_A, \quad \overline{\overline{k}}_m = b_0 + \sum_{j=1}^{N_k} b_j \overline{\overline{Q}}_{j,m} + \varepsilon_k, \tag{2}$$

where the index $m = 1,12$ denotes the month and the double overbars indicate multi-year averages of monthly mean quantities. In PSB05, A_m and k_m were derived from once-daily (1300 local time) observations at each station over the present period, while output fields from a coupled atmosphere–ocean GCM (ECHAM4/OPYC3) were used as predictors (the authors first validated these against NCEP/NCAR reanalysis fields). As predictors, PSB05 selected the multi-year monthly mean maximum horizontal gradient in sea-level pressure $PG_{\max}$ (indicative of the wind magnitude according to the pressure-slope diagnostic, as determined from the 8 grid values adjacent to the closest grid point), relative vorticity on the 500 hPa surface RV_{500} (a proxy for vertical motion), and its standard deviation $\sigma(RV_{500})$ (a measure of "storminess"). The same predictors were used for both A and k. In Eq. (2), a_j and b_j are thus monthly mean, station-specific regression coefficients found by an error minimization procedure (e.g., linear least-squares fitting) to the 12 monthly values A_m in a $(N_A + 1)$-dimensional space.

We conducted an analogous seasonal downscaling exercise over the BC region. Like Scandinavia, the BC region is characterized by complex topography and significant oceanic influence. Aside from the different domain, our approach differs from PSB05 in several respects, none of which should substantially affect our evaluation of the robustness of the seasonal downscaling method used in this earlier paper. First, instead of using GCM model output variables as predictors, which are unconstrained by observations, we used NCEP-2 reanalysis fields, which should have smaller biases than GCM fields. Second, instead of employing RV_{500} as a proxy for vertical motion at the synoptic scale as in PSB05, we instead used vertical motion at 500 hPa, ω_{500}, directly. Thus, ω_{500} and its standard deviation, $\sigma(\omega_{500})$, were chosen instead of RV_{500} and $\sigma(RV_{500})$. These fields along with $PG_{\max}$ comprise the basic predictor set for our regressions using the seasonal methodology. According to the simple pressure-slope view of local wind behaviour, one might expect that whereas the mean wind (and therefore A) should be related to $PG_{\max}$, the skewness of the distribution (roughly proportional to the inverse of k) should be more closely linked to variability in the wind or its components. Finally, we carried out the analysis for two different sampling frequencies: the full 24-h sampling reflected in the homogenized monthly mean data, and once-daily sampling (at 1300 local time, as in PSB05) using the unhomogenized hourly wind speed data. In the former case, the monthly standard deviation of W was assumed to be the same as in the unhomogenized data. The quality of the multi-linear fit at each station is gauged by the coefficient of determination R^2 and probability p associated with the null hypothesis of uncorrelated data, as computed by the standard F test (Wilks 1995).

For both A and k, significant correlations are found at the majority of stations (14 out of 20) at the $P < 0.05$ level, with a corresponding mean $R^2 = 0.82$ for A and 0.73 for k over stations with significant correlations (recall that $m = 12$ in the seasonal downscaling method). For A, ω_{500} and $\sigma(\omega_{500})$ account for the majority of the variance at stations with significant correlations (Fig. 4 and 5), with a lesser contribution from $PG_{\max}$ (Fig. 3). The best single predictor for k is $\sigma(\omega_{500})$, followed by ω_{500} (not shown). $PG_{\max}$ is a good predictor of either A or k at only 8 of 20 stations. Moreover, only 11 of the 20 stations display significant correlations for both A and k. The results for once-daily sampling of W are qualitatively similar, but the R^2 values are on average $\sim$10% smaller, reflecting the decreased sampling frequency.

The results of the seasonal regressions might be interpreted, as they were in PSB05, as affirming the explanatory power of the selected predictor fields with respect to the observed wind properties at the majority of stations. This straightforward interpretation must be viewed with some caution, however, due to the central role of seasonality in the downscaling approach. The object of the regression fitting is ostensibly to extract a unique relationship between, e.g., A, and the fields P_j *at a particular station*. Since the dominant mode of variability reflected in the monthly means of both predictors and predictands is the annual cycle, the resulting regressions essentially relate their respective annual cycles. Although this was pointed out over 20 years ago by Wigley et al. (1990) in the context of downscaling surface temperature, it seems not to be generally recognized. Hence, we present a number of demonstrations in the present context to emphasize the point.

The annual cycle of a specific predictor j may be fit to a first approximation by a sinusoidal function of the form $S_j = S_{0,j} \sin[(2\pi m/12) + \varphi_j]$, $m = 1, 12$. The results of the fits at each station, for each of the 3 predictors, are shown

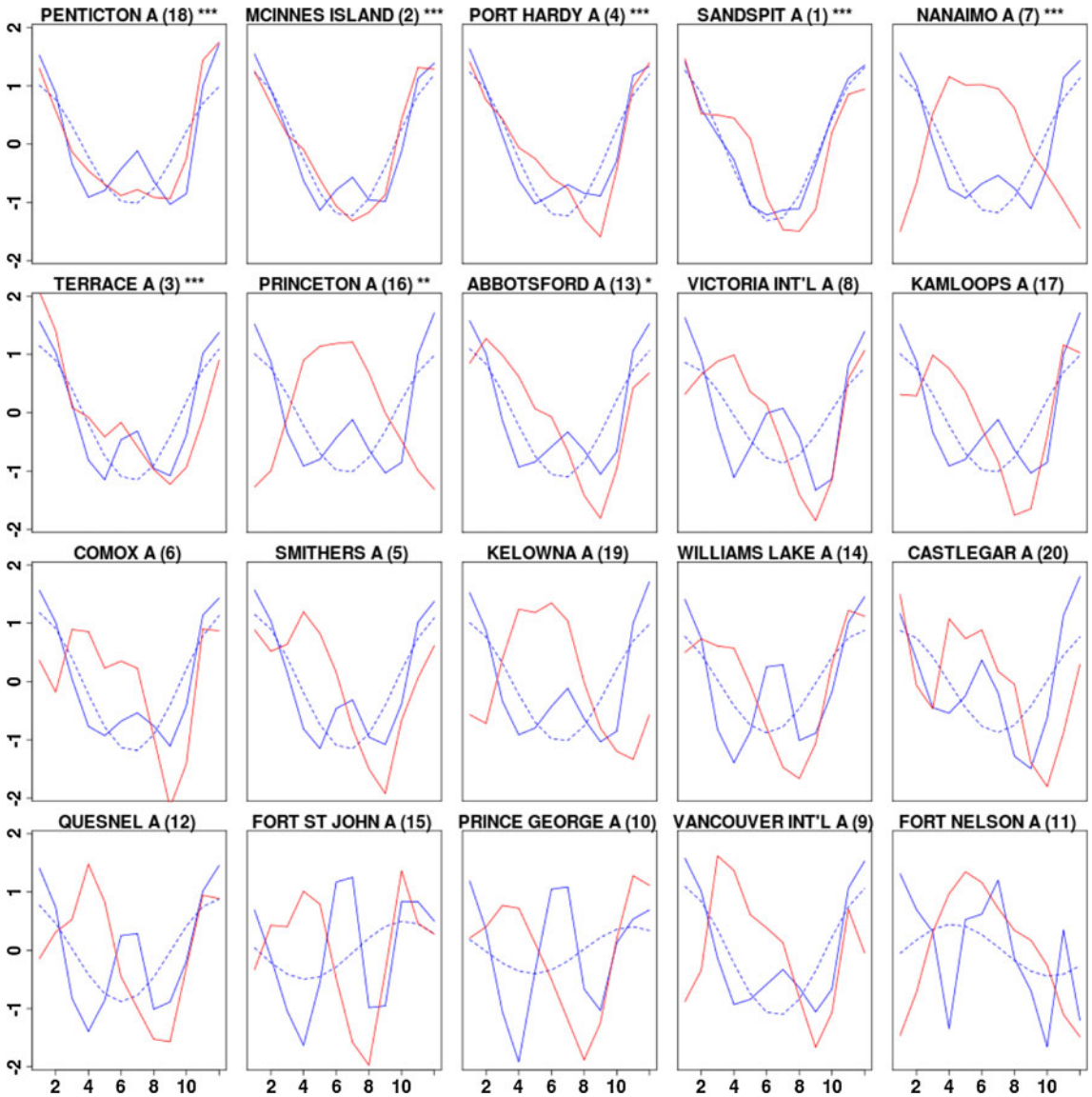

Fig. 3 Sinusoidal fits (dashed blue curves) to monthly mean PG_{max} (solid blue curves) at all stations. In this and the following two figures, the predictor values are normalized to an annual mean value of zero and standard deviation of unity. Red curves are the monthly mean Weibull A parameter fitted to data at each station. Stations are identified by name and ordering in Fig. 1, and asterisks indicate the significance level of the correlation found: *** = 99.9% significance, ** = 99% significance, and * = 95% significance

in Figs. 3, 4, 5. The figures show that at the reanalysis grid cells corresponding to most stations, the predictors are well fit by a sinusoid. The annual cycle is also apparent in the predictand A, with the exception of several stations where it displays a double-peaked structure associated with the semi-annual cycle (the results are similar for k, but are omitted for brevity). The seasonality of A at the coastal stations, with the largest wind speeds in winter, is in accord with the documented behaviour of mean wind at other coastal stations (Lange 2003) and at offshore buoys (Merryfield et al. 2009). At stations where the regression fit is poor, the predictand and/or predictors depart strongly from sinusoidal behaviour (bottom panels of Figs. 3, 4, 5).

The regressions of A and k against each single predictor were repeated with $S_{j,m}$ in place of $P_{j,m}$ on the right-hand side of Eq. (2), yielding the correlation coefficients r_S (here we use lowercase r to distinguish single-variable from multivariate regressions). Using single predictors clarifies the relationship between predictors and predictands by avoiding colinearity among predictors. For $\sigma(\omega_{500})$, there is no significant difference between r and r_S at the majority of stations. For the other two predictors, r_S is typically larger than r, especially when k is the predictand. *Thus, the overall quality of the regressions is closely tied to their ability to predict the annual cycle of the local A and k parameters.*

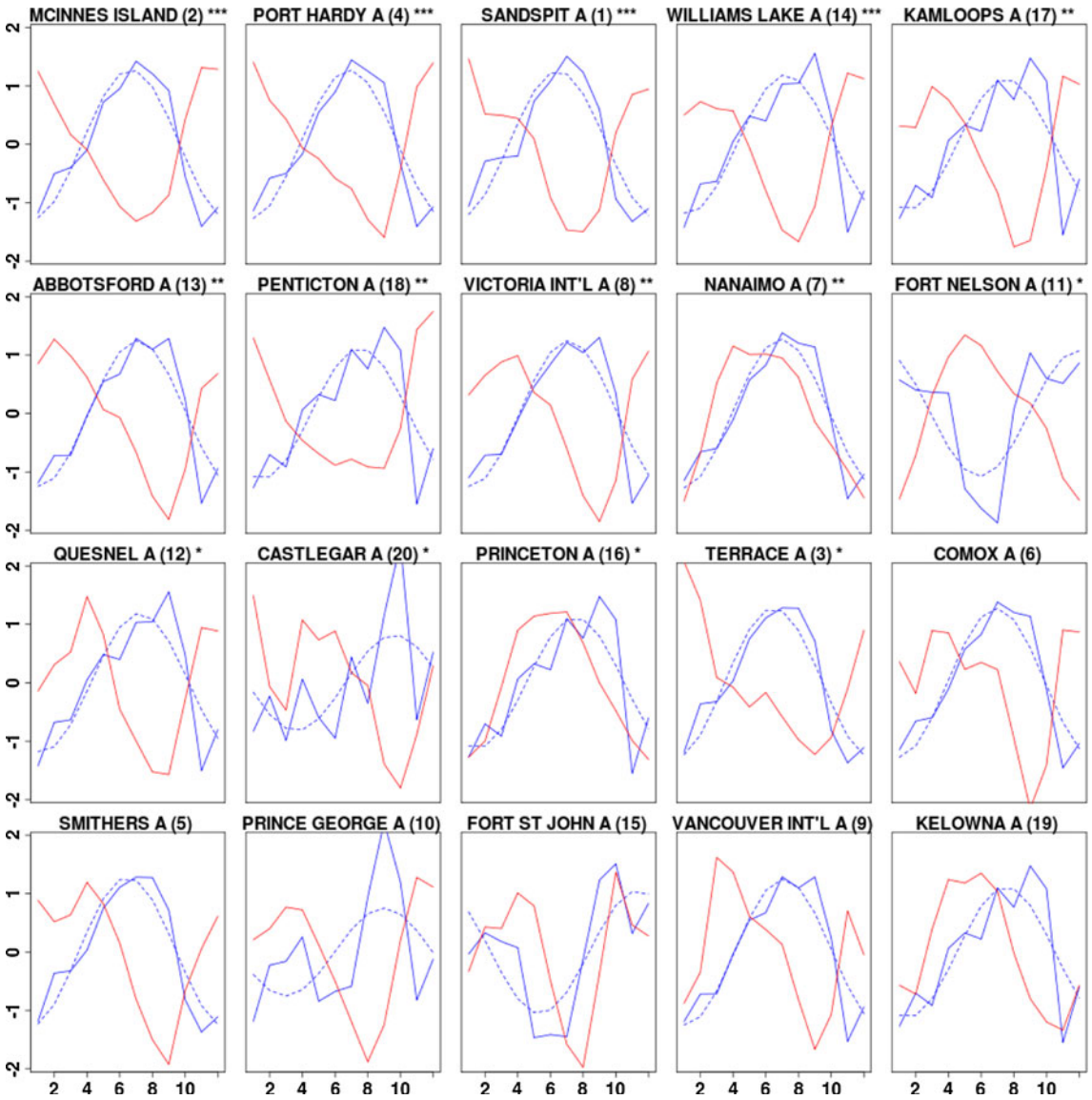

Fig. 4 Same as Fig. 3, but for monthly mean ω_{500}

The concern regarding the seasonal methodology may also be expressed in terms of the number of statistical degrees of freedom available in the multilinear fit. For an exactly sinusoidal predictand with only two degrees of freedom (amplitude and phase), a regression involving two or more exactly sinusoidal predictors has a coefficient of determination R^2 equal to unity, while for a single sinusoidal predictor, $r^2 = \cos^2\theta$, where θ is the phase difference between predictand and predictor (see Appendix). While the actual predictors and predictands are not pure sinusoids, Figs. 3, 4, 5 show that nearly sinusoidal predictors and predictands are associated with r^2 values closer to unity. Moreover, the small number of observations entering the regressions ($m = 12$) raises the concern of overfitting. Application of the Akaike information criterion (Burnham and Anderson 2002) to the fits indicates that at most stations, there is little to be gained by adding a third predictor (in most instances, $PG_{\max}$). At certain stations, one finds $R^2 \gg r^2$ when the latter is not statistically significant for any single predictor. This feature is a hallmark of overfitting.

In light of the above, the value of the derived regression relations in the context of future climate projections needs to be regarded skeptically. Since the annual cycle is a manifestly large-scale feature present in nearly all climate variables, including local quantities, this limits the scope of the downscaling exercise. As emphasized by Wigley et al. (1990), if differences in A_m between stations over the region in any given month are smaller than the magnitude of the seasonal cycle in A, then the coefficients a_j are likely

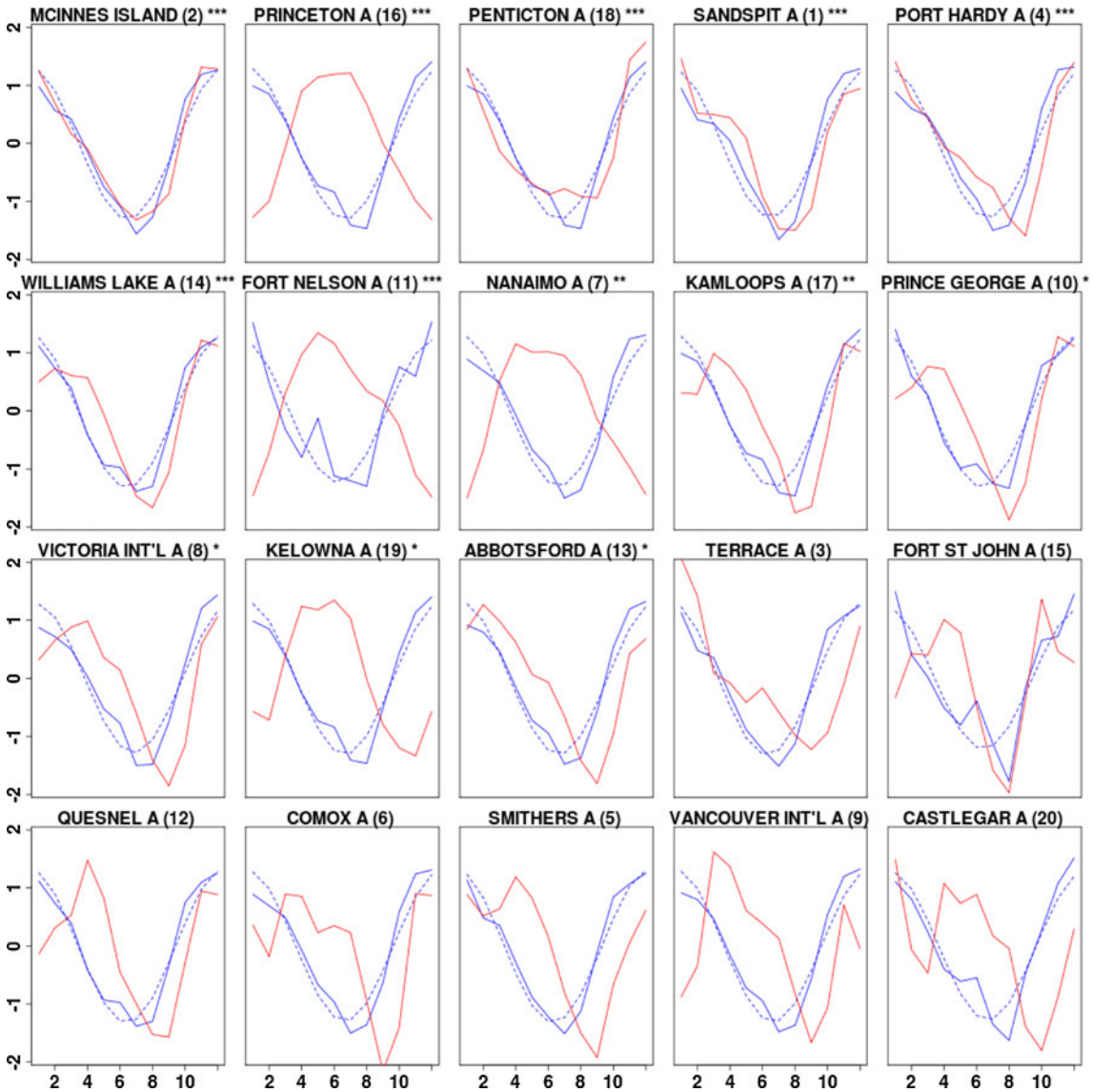

Fig. 5 Same as Fig. 3, but for monthly mean $\sigma(\omega_{500})$

to be more indicative of the common seasonality between A and P_j than of any truly local differences. Specifically, if the seasonal amplitudes of A and P_j are δA and δP_j, respectively, then it follows that the regression coefficients $a_j \sim (\delta A)/(\delta P_j)$, assuming ε_A is small. The same argument clearly holds for k.

Some other features of Figs. 3, 4, 5 are worthy of further comment. Of the three predictors, the fit is poorest for $PG_{\max}$, which displays a small secondary peak in summer at all but one station (Fig. 3). Also, a few stations (those in the bottom rows of Fig. 3 and 4) show oscillatory behaviour in $PG_{\max}$ and ω_{500} on a sub-annual (seasonal) timescale, which cannot be fit by an annual sinusoid. At stations with the largest single-variable r^2 (top row of Figs. 3, 4, 5), A is generally in phase with $PG_{\max}$ and $\sigma(\omega_{500})$ (excepting the Princeton station, and Fort Nelson for $\sigma(\omega_{500})$), and 180° out of phase with ω_{500}. The results for the other predictand k (not shown) are similar.

As a means of illustrating the difficulty of detecting interstation differences in the local surface winds using the seasonal regressions, we conducted a Monte Carlo simulation in which the predictands A_m and k_m at one station were randomly reassigned to another station, and the regression fit repeated using the original set of three predictors $P_{j,m}$. If a significant portion of the explained variance in the original multiple linear regressions arises from local features of the wind field, then regressing a set of predictors at one station against a predictand from any other station should give a considerably smaller R^2 value. This random station swap was performed 2,000 times, yielding the distributions of R^2 plotted in Fig. 6. Not surprisingly, given the random selection procedure, the

distributions for both A and k are roughly gaussian. The mean R^2 values obtained over all stations from the original regressions for A and k are shown as vertical dashed lines in Fig. 6. In both cases, the original R^2 value lies near the peak of the randomly swapped distribution, indicating that approximately half of the randomly swapped correlations are larger than the original. These results clearly demonstrate that local environmental conditions at the stations make a minor contribution, if any, to the regression relations derived from seasonally varying station and large-scale reanalysis data. Repeating the analysis using once-daily sampled data gives the same qualitative conclusions.

The above results highlight clear caveats in the use of climatological monthly mean fields in the downscaling procedure, e.g., as used by PSB05, when the objective is to derive regressions containing local station-level information. Predictors with strong annual cycles from the other side of the globe could yield skillful predictions in this approach, when in fact such apparent skill arises due to the small number of statistical degrees of freedom in the seasonal cycle. In the next section we outline a modified procedure using deseasonalized predictors and predictands to perform the downscaling.

3.2 Use of interannual variations

In order to avoid the dominant effect of seasonality on the wind regressions, we reconsidered the same wind speed data with a focus on their interannual variability. Figure 7 compares the seasonal and interannual variability of surface wind speed at two representative stations, Vancouver and Prince George. The left-hand panels show the distribution of W by month averaged over all years (i.e., monthly climatology), while the right-hand panels show the distribution of W by year averaged over all months. Monthly mean wind speeds from the adjusted data set of Wan et al. (2010) were used to construct both types of plot. Interannual variability in W (horizontal variation of mean values in the right-hand panel) is comparable in magnitude to the seasonal variation (horizontal variation of means in the left-hand panel) at Vancouver, but is about a factor of two smaller at Prince George (lower panels). Thus, although the interannual variability in mean wind is generally smaller than the seasonal cycle, the regression-based approach of Sect. 2.3 should still be appropriate to ascertain the relative impact of different predictors on the behaviour of A and k.

In the interannual methodology, we write the relevant transfer functions at a given station as:

$$\begin{aligned} \overline{A}_{i,m} &= a_{0,m} + \sum_{j=1}^{N_A} a_{j,m}\overline{P}_{i,j,m} + \varepsilon_A, \\ \overline{k}_{i,m} &= b_{0,m} + \sum_{j=1}^{N_k} b_{j,m}\overline{Q}_{i,j,m} + \varepsilon_k, \end{aligned} \tag{3}$$

where $m = 1, 12$ is the month index, $i = 1, 28$ is the year index, and j is the predictor index. The single overbar on A and k in Eq. (3) indicates that individual monthly means are used (e.g., $\overline{A}_{1,2}$ refers to February 1979), rather than multi-year means of a given month as in Eq. (2). The prediction of individual months' wind statistics is possible in this approach since both predictors and predictands are observation-based.

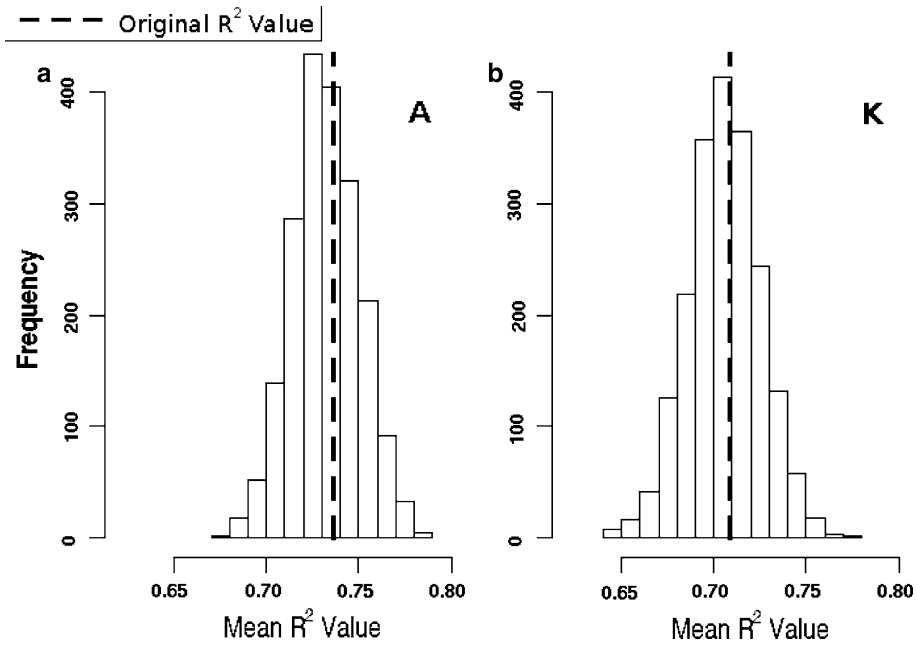

Fig. 6 Distribution of R^2 values (mean over all stations) using the seasonal downscaling method and the standard 3-predictor set, with random swapping of predictands among the stations. Results for both A (left) and k (right) are shown. The dashed line shows the original (non-randomized) mean value of R^2 computed from all 20 stations

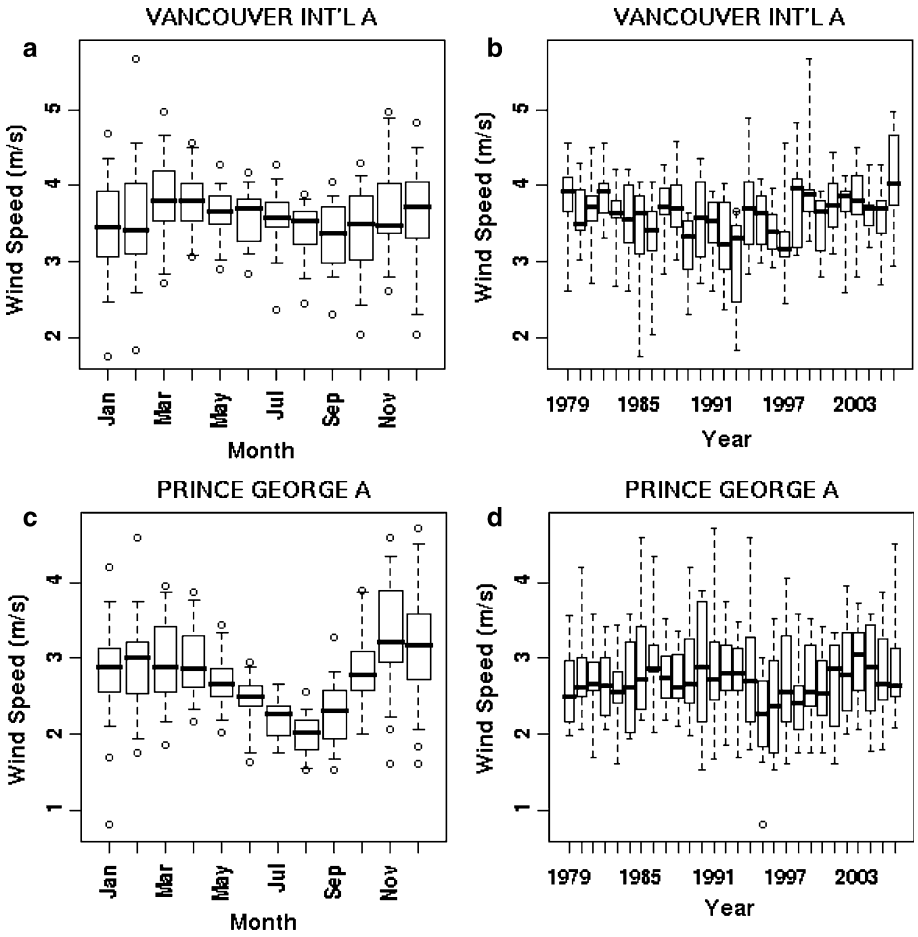

Fig. 7 Comparison of seasonal (left) versus interannual (right) variability in surface wind speed at Vancouver (top) and Prince George (bottom). Data plotted are monthly mean wind speeds from the adjusted historical data set of Wan et al. (2010). Boxes demarcate the 25th and 75th percentiles, while error bars show the 5th and 95th percentiles. Values lying outside this range are shown as open circles

Certain advantages are immediately evident in the interannual methodology: (1) By developing regression models for individual months, seasonal differences can be distinguished; (2) The number of regressed points for a given month is increased to $N = 28$ (1979–2006), while aggregating into seasons (the procedure we followed) gives $N = 3 \times 28 = 84$, greatly reducing the risk of overfitting; (3) Autocorrelation has also been greatly reduced, increasing the number of statistical degrees of freedom; (4) Use of cross-validation is possible, wherein the regression coefficients for a given season are first determined from a portion (typically 3/4) of the data, and then validated against the reminder of the records. This procedure was then repeated many times on different subsets of the data.

Finally, the effect of including several new predictor fields in the regressions, beyond those considered by PSB05, was explored. The additional fields were the zonal and meridional wind components at 500 hPa, U_{500} and V_{500}, and the temperature difference between 1,000 and 700 hPa, $T_{1,000–700}$. The motivation for including the wind components aloft is that they may have a driving influence on the corresponding surface components (and are also equivalent to the horizontal pressure gradient aloft, through geostrophy). In the absence of higher resolution information, $T_{1,000–700}$ might give some indication of lower tropospheric stability. In each season, predictors were added one at a time at each station, until the addition of a predictor provided no substantial improvement in the mean cross-validated R^2 over all stations. We term the resulting predictor set "optimal," although it should be noted that the selection of predictors is not itself subject to cross validation. Finally, some care was taken to avoid choosing correlated predictors (e.g., ω_{500} and $\sigma[\omega_{500}]$), which can degrade the quality of the fits.

The results of the regressions using the interannual approach with optimal predictors are summarized in Table 2. In our implementation of the method, optimal predictors are the same at every station, but vary according to season (Table 2, bottom). The use of optimal in contrast to standard predictors improves the quality of the regression fits for A, but the results for k are largely unchanged. This is illustrated in Fig. 8, in which R^2 for optimal predictors is plotted against R^2 for standard predictors for A and k at all stations. The overall increase in cross-validated R^2 (CV R^2) for both A and k is about 20% using optimal versus standard predictors (Fig. 8a–c), except for

Table 2 Results of interannual regressions (multilinear R^2 values) for Weibull A and k parameters with hourly sampling and using optimal predictors for each season: winter (DJF), spring (MAM), summer (JJA), and fall (SON)

ID	Station	Predictand: A									Predictand: k								
		DJF		MAM		JJA		SON		ANN	DJF		MAM		JJA		SON		ANN
		Raw	CV	Raw	CV	Raw	CV	Raw	CV	CV	Raw	CV	Raw	CV	Raw	CV	Raw	CV	CV
2	McInnes Island	0.74	0.70	0.50	0.42	0.34	0.21	0.72	0.67	0.50	0.39	0.29	*0.10*	*0.01*	0.31	0.13	0.19	0.08	0.13
4	Port Hardy	0.50	0.45	0.48	0.41	0.13	*0.03*	0.80	0.76	0.41	0.31	0.23	*0.10*	*0.01*	0.17	*0.05*	0.24	0.14	0.11
6	Comox	0.62	0.57	0.30	0.21	0.29	0.18	0.54	0.47	0.36	0.21	0.13	0.21	0.10	0.28	0.17	0.23	0.13	0.13
9	Vancouver Int'l	0.74	0.71	0.19	0.08	*0.08*	*0.01*	0.60	0.55	0.34	0.21	0.12	0.24	0.12	0.17	0.07	0.29	0.18	0.12
8	Victoria Int'l	0.42	0.35	0.21	0.11	0.30	0.19	0.65	0.59	0.31	*0.03*	*0.06*	*0.11*	*0.02*	*0.09*	*0.01*	0.14	*0.05*	0.04
18	Penticton	0.44	0.39	0.28	0.18	*0.07*	*0.00*	0.58	0.52	0.27	0.22	0.15	*0.04*	*0.02*	0.19	0.09	*0.08*	*0.01*	0.07
15	Fort St. John	0.37	0.29	0.31	0.23	0.48	0.40	0.27	0.17	0.27	*0.08*	*0.02*	*0.12*	*0.02*	*0.04*	*0.01*	*0.09*	*0.01*	*0.02*
17	Kamloops	0.23	0.15	0.23	0.14	0.26	0.13	0.63	0.57	0.25	0.12	*0.03*	0.30	0.19	0.14	*0.04*	0.49	0.42	0.17
1	Sandspit	0.40	0.31	0.37	0.28	0.25	0.14	0.31	0.20	0.23	0.18	0.09	0.28	0.17	0.35	0.24	0.49	0.39	0.22
14	Williams Lake	0.39	0.33	0.24	0.15	*0.13*	*0.03*	0.49	0.41	0.23	0.30	0.23	0.14	*0.03*	*0.09*	*0.01*	0.16	0.07	0.08
10	Prince George	0.43	0.36	0.23	0.13	0.22	0.11	0.35	0.26	0.21	0.36	0.28	*0.11*	*0.02*	0.24	0.13	*0.10*	*0.02*	0.11
13	Abbotsford	0.17	*0.06*	0.34	0.24	0.15	*0.05*	0.52	0.41	0.19	0.11	*0.03*	0.14	*0.05*	*0.08*	*0.01*	*0.09*	*0.01*	0.02
5	Smithers	0.36	0.29	0.13	*0.03*	0.24	0.13	0.38	0.29	0.19	0.26	0.18	*0.06*	*0.01*	0.32	0.21	0.18	0.08	0.12
3	Terrace	0.41	0.34	0.22	0.12	0.27	0.14	0.23	0.12	0.18	0.25	0.17	0.17	*0.06*	*0.10*	*0.01*	*0.07*	*0.01*	0.06
7	Nanaimo	0.35	0.28	*0.11*	*0.02*	0.28	0.17	0.31	0.20	0.17	*0.08*	*0.01*	0.32	0.20	0.21	0.10	0.27	0.17	0.12
16	Princeton	*0.09*	*0.02*	0.32	0.22	0.21	0.10	0.42	0.33	0.17	*0.06*	*0.01*	0.21	0.10	0.15	*0.04*	0.25	0.15	0.08
11	Fort Nelson	0.18	0.10	0.24	0.14	*0.13*	*0.03*	0.28	0.17	0.11	0.16	0.09	0.20	0.09	0.15	*0.04*	*0.07*	*0.01*	0.06
12	Quesnel	0.23	0.14	*0.05*	*0.01*	*0.11*	*0.01*	0.30	0.20	0.09	0.20	0.12	*0.08*	*0.01*	0.14	*0.04*	0.14	*0.05*	0.05
19	Kelowna	0.18	0.10	*0.02*	*0.04*	*0.11*	*0.01*	*0.11*	*0.01*	0.04	0.19	0.11	0.21	0.10	*0.10*	*0.01*	*0.08*	*0.01*	0.06
20	Castlegar	0.10	*0.03*	0.16	*0.05*	0.17	*0.04*	*0.06*	*0.01*	0.03	*0.03*	*0.02*	0.16	*0.05*	*0.10*	*0.01*	0.21	0.10	0.05
Mean		0.37	0.30	0.25	0.16	0.21	0.11	0.43	0.35	0.23	0.19	0.12	0.17	0.07	0.17	0.07	0.19	0.10	0.09
Standard deviation		0.19	0.20	0.13	0.12	0.10	0.10	0.20	0.22	0.12	0.11	0.09	0.08	0.06	0.09	0.07	0.12	0.12	0.05
Minimum		0.09	0.02	0.02	0.01	0.07	0.00	0.06	0.01	0.03	0.03	0.01	0.04	0.01	0.04	0.01	0.07	0.01	0.02
Maximum		0.74	0.71	0.50	0.42	0.48	0.40	0.80	0.76	0.50	0.39	0.29	0.32	0.20	0.35	0.24	0.49	0.42	0.22
Optimal predictors		$T_{1,000–700}$		PG_{max}		$T_{1,000–700}$		$T_{1,000–700}$			$T_{1,000–700}$		$T_{1,000–700}$		$T_{1,000–700}$		U_{500}		
		PG_{max}		ω_{500}		$\sigma(\omega_{500})$		U_{500}			PG_{max}		$\sigma(\omega_{500})$		$\sigma(\omega_{500})$		V_{500}		
		U_{500}		$T_{1,000–700}$		ω_{500}		V_{500}			U_{500}		U_{500}		U_{500}		PG_{max}		
				U_{500}		V_{500}							V_{500}		V_{500}		$T_{1,000–700}$		
						PG_{max}							PG_{max}		PG_{max}				

Italic values indicate non-significant correlations (i.e., $P > 0.05$). "Raw" and "CV" refer to regressions without and with cross-validation, respectively. Stations are ordered according to highest annual mean cross-validated R^2 value for A. Optimal predictors for each season and predictand appear at the bottom of the table

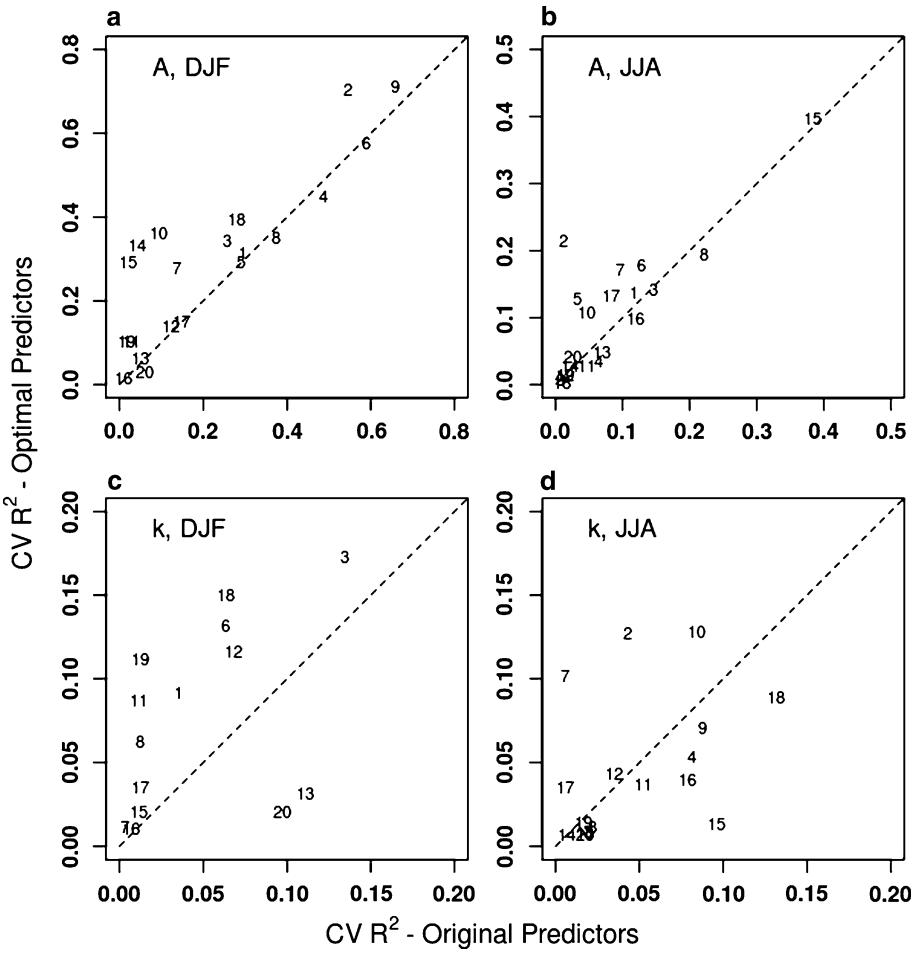

Fig. 8 Scatter plots of cross-validated R^2 for optimal (ordinate) versus standard (abscissa) predictor sets and for predictands A (top) and k (bottom). Winter (DJF) is shown at left, summer (JJA) at right. Individual points are numbered by station ID from Fig. 1; Table 1

k in summer (Fig. 8d), when there is no improvement. In fall and winter, more of the stations have CV R^2 values for *A* exceeding 0.5 for the optimal predictor sets, with the "best" station having an annual mean CV $R^2 = 0.58$. In autumn (SON), the optimal predictors are (in order of variance explained) $T_{1,000–700}$, U_{500}, and ω_{500}, while in DJF they are $T_{1,000–700}$, PG_{max}, and U_{500}. Once again the R^2 values for *k* are much smaller than for *A*, indicating little or no predictive ability for this Weibull parameter (Table 2).

In Table 2, the values of both standard R^2 and CV R^2 are tabulated. The difference between the two indicates the extent to which the former values are inflated by overfitting. Examining the results for *A* first, all but three of the stations have significant R^2 in SON or DJF, although $R^2 > 0.5$ at only three of 20 stations in DJF (7/20 stations in SON). The correlations are less robust in MAM and JJA, and in all seasons using cross validation, indicating some sensitivity to the exact time period used. The results for *k* are much poorer than for *A*, with the "best" station having an annual mean CV $R^2 = 0.13$, versus $R^2 = 0.50$ for *A*.

Although the quality of the regression fits using the interannual method is not striking, one can nevertheless demonstrate that local wind characteristics are now being captured. Figures 9 and 10 show the results of the random station swapping exercise described in Sect. 3, now using the interannual predictands and the same three predictors as in the seasonal regressions. In contrast to the results of Sect. 3, one now sees that the original regression is superior to the vast majority of randomly swapped combinations in all seasons except JJA (consistent with the generally weak downscaling predictive skill in this season), indicating that the regression indeed captures some aspects of the local wind climatology. Put differently, this result clearly demonstrates that interannual fluctuations tend to be more meaningfully connected with local atmospheric variability than seasonal variations, a sensible result given that the latter are of solar-terrestrial origin.

4 Downscaling of surface wind variations using non-local predictors

While the above results indicate that some characteristics of local wind speed are being captured in the interannual regressions using predictor values at the closest reanalysis

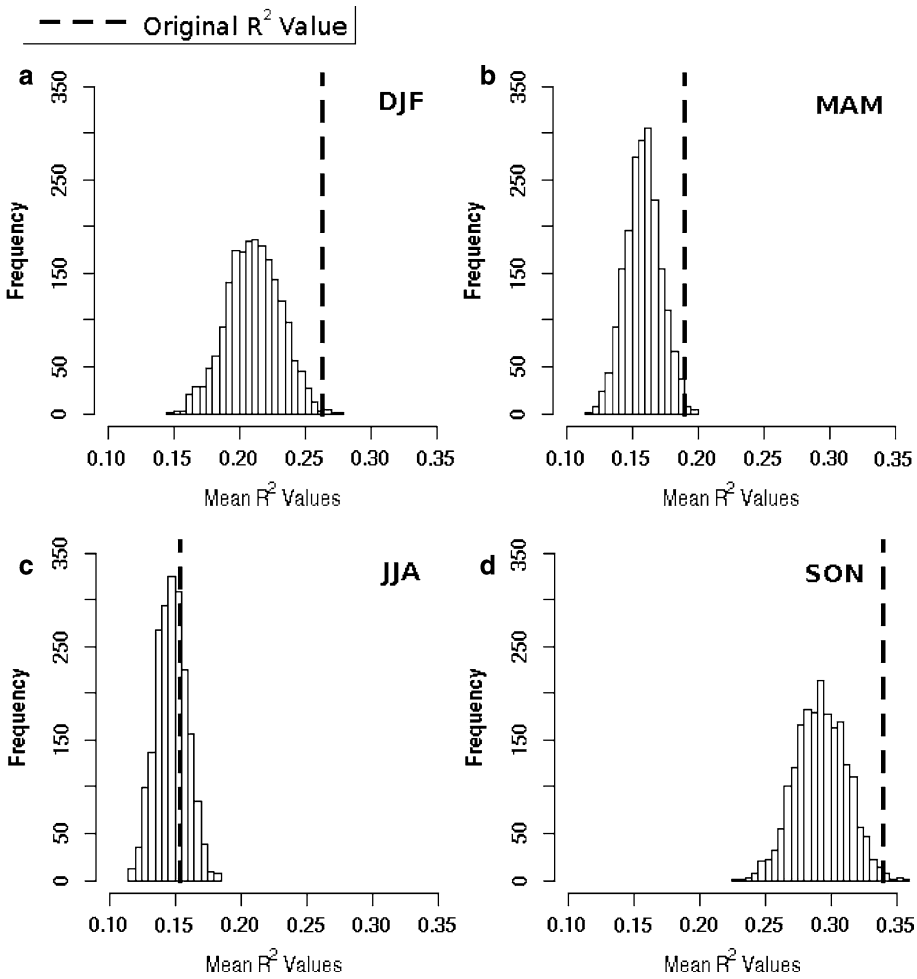

Fig. 9 Distribution of standard R^2 values using the interannual downscaling method and the standard 3-predictor set, with random swapping of predictands amongst the stations. Results are for the Weibull A parameter. The dashed line shows the original (non-randomized) mean value of R^2 computed from all 20 stations

grid cell, the overall low R^2 values imply that much of the variance in the local surface wind speed is still unexplained. One can now ask: how much of the variance in W at a given station is due to predictor behaviour at some distance from the station? This is a reasonable question since it is known, e.g., that pressure extrema at the surface are displaced horizontally from those aloft due to the vertical gradient of temperature (Barry and Chorley 1977). Also, since predictive information may be carried in large-scale structures of variability, focusing on these may filter out local "noise" that degrades prediction skill.

To examine this question, we carried out the regressions using predictor values over a much larger region, spanning 180°–90°W and 30°–70°N, instead of at the closest grid point only. Spatial maps of the multi-year mean predictors at 500 hPa along with mean sea level pressure in DJF are shown in Fig. 11, while the resulting correlation maps of each predictor with the A parameter for two stations are presented in Figs. 12 and 13. The stations chosen, Vancouver and Fort Nelson, are located at opposite corners of British Columbia, approximately 1,000 km apart. The chosen predictors are those from the extended set, omitting $PG_{\max}$ and $T_{1,000-700}$, which as local gradients are expected to have a more short-range influence. Each of Figs. 12 and 13 shows the pattern of correlation r for single-variable regressions of the Weibull A parameter against the indicated predictor field, the corresponding multivariate regression R^2, and at lower right, the wind rose for the station in DJF. Note that while panels a to d in each figure show the correlation of predictor with the *predictand* A, i.e., corr(P_j, A), panel e displays the correlation of multiple predictors with the *prediction*, i.e., corr(A', A), expressed as R^2, which is always positive.

For both A and k, the maximum CV R^2 values over the entire domain computed for each station tend to be about 0.05–0.1 units larger, over all seasons, than those found using the optimal, local predictor set in Table 2. Inspection of Figs. 12 and 13 (and the maps for the remaining stations, not shown) shows that in no case does the highest multilinear R^2 value occur at the nearest grid box to the indicated station. However, it can be nearby, as in the case of Vancouver (Fig. 12e). In the single predictor maps there exist regions of negative, as well as positive correlation, indicating that A and the indicated variable at that station

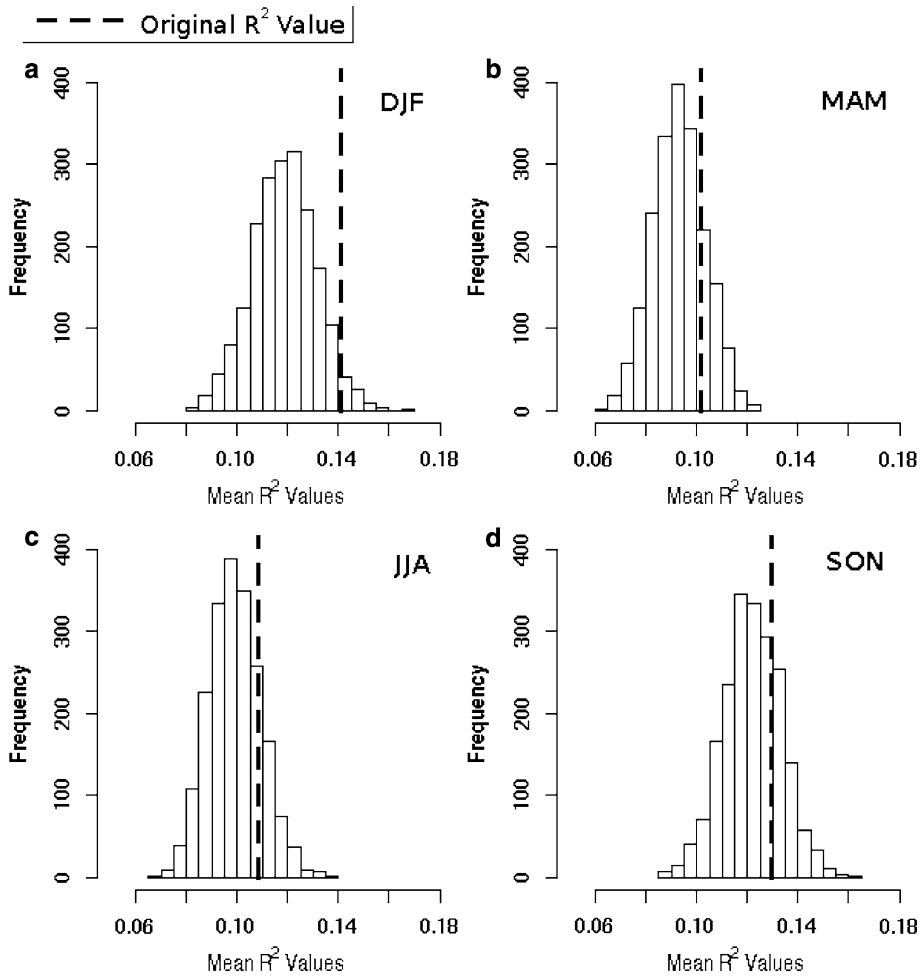

Fig. 10 Same as Fig. 9, but for the Weibull k parameter

vary in the opposite sense. In most cases, the loci of largest r for single predictors are located offshore over the Pacific Ocean, or if onshore, near the coast. This is true even for the Fort Nelson station, which is located over 500 km from the coast (Fig. 13). Since disturbances of the mid-latitude jet stream propagate from west to east on average, this relationship of surface winds with the upstream state of the atmosphere aloft is not surprising (Barry and Chorley 1977). At Fort Nelson in DJF, the predictability of A is much improved by using remote predictors: the CV $R^2 = 0.59$ compared to only 0.10 using predictors at the closest grid point.

Figure 11c shows the mean pattern of wind speed and direction at 500 hPa; winds are generally southwesterly offshore, shifting to northwesterly over the BC interior (following the climatological ridge over western North America). The stations under consideration are located in the narrow transition region between these two patterns. The large-scale, dipolar patterns of positive and negative correlation observed for the 500 hPa wind components in Figs. 12a,c and 13a,c likely result from interannual and interdecadal variability of the Pacific storm track, which shifts equatorward and extends eastward in El Nino years, and vice versa in La Nina years (Chang et al. 2002; Hanawa et al. 1996). To understand why the dipolar correlation patterns are of opposite sign in the two maps, we plotted the A values in DJF at both stations over the entire period (not shown), noting an anti-correlation between the two time series ($r^2 = 0.36$, $P = 10^{-9}$, $N = 84$). On the other hand, inspection of interannual U_{500} anomalies reveals a meridional dipole with fluctuations of opposite sign in the northern and southern parts of the domain, the result of the interannual shift in the storm track latitude. Together, these explain the opposite signs of the respective correlation patterns.

The correlation patterns for ω_{500} and $\sigma(\omega_{500})$ are more complex, but again are roughly opposite at the two stations (Figs. 12b,d and 13b,d). For example, the region of negative correlation surrounding Vancouver indicates an increase in mean surface wind speed during periods of predominant uplift, which is consistent with convergent flow near the surface.

At the surface, easterly winds are most frequent at Vancouver in DJF (Fig. 12f), implying a reversal of wind direction near the surface from that aloft. This is consistent with a low pressure trough in the Gulf of Alaska (Fig. 11d), which

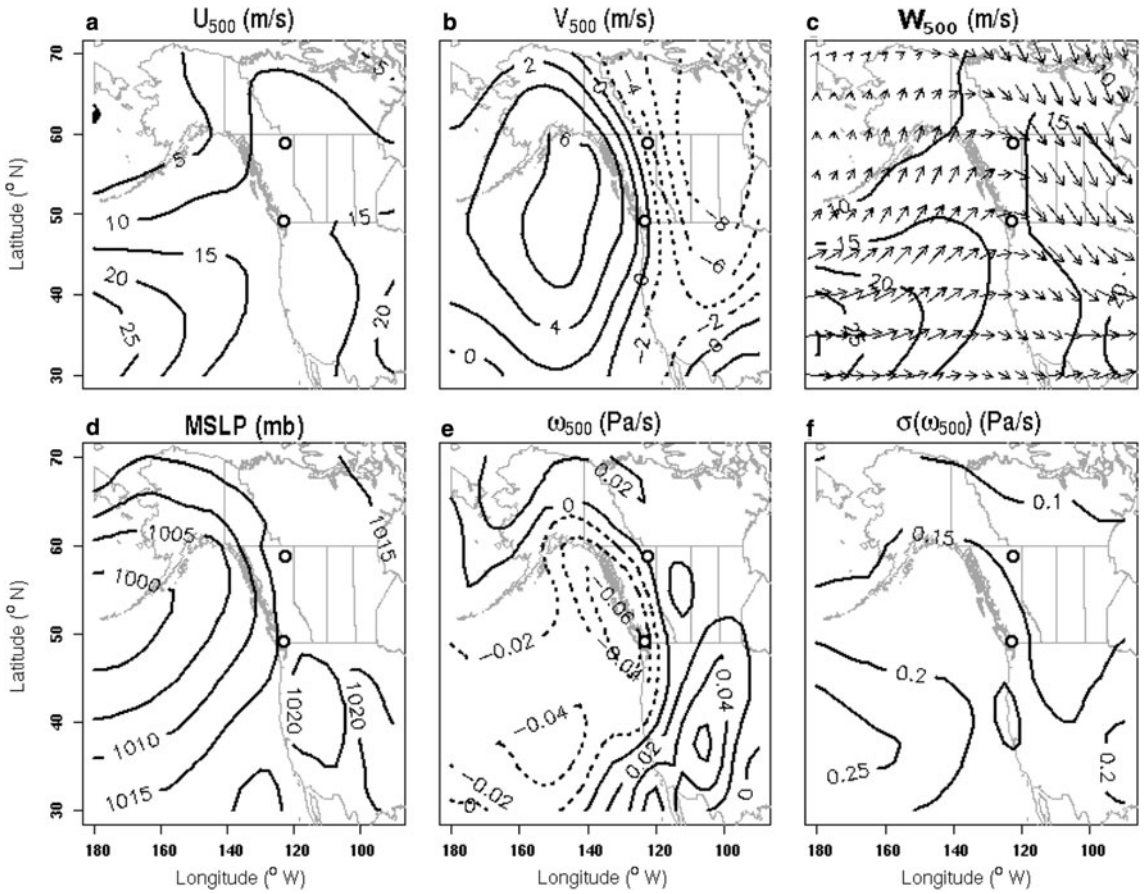

Fig. 11 Structure of indicated NCEP-2 fields over the analysis domain: a U_{500}; b V_{500}; c wind speed (and direction, indicated by arrows) at 500 hPa, $\boldsymbol{W}_{500}$; d mean sea level pressure; e ω_{500}; f $\sigma(\omega_{500})$. Each field is a DJF mean over 1979–2006. Vectors in c show the wind speed direction at 500 hPa. Eastward and northward winds and descending motion are positive. Open circles on each panel show the locations of Vancouver (lower) and Fort Nelson (upper)

favours the development of southeasterly winds along the pressure gradient, channeled by the Coast Range directly north of Vancouver into a more easterly direction. At Fort Nelson, surface winds are predominantly westerly (Fig. 13f), in better agreement with the winds aloft (Fig. 11c), but considerably weaker than at Vancouver. The weak correlations found for individual predictors at the closest NCEP-2 grid point to Fort Nelson are consistent with the location of the peak R^2 some distance to the northwest (Fig. 13e).

In summary, the examination of large-scale predictor fields and the associated correlation patterns with A for individual stations suggests that a significant portion of the observed variance in mean wind speed at certain stations in BC is attributable to monthly time scale variability in the chosen predictors. However, quantifying the improvement in predictive power is complicated by the fact that the various predictors are likely to have some degree of covariance, as mentioned in Sect. 3.2. A more systematic means of avoiding this covariance is a principal component analysis decomposition of the predictors, a technique we apply to both surface wind speed and components in Paper II.

5 Discussion and conclusions

All statistical downscaling methods presume the existence of a relationship between the large-scale atmospheric flow and local weather or, in the longer term, climate. This relationship is typically calibrated using input data from either large (e.g., reanalysis products) or small scales (e.g., station data), or both, and its robustness may be assessed a posteriori by validation against data from a time period not included in the calibration. Before applying the downscaling relationship in some other context (e.g., future large-scale GCM projections), it is essential to verify that the relationship holds using historical observations.

In this paper we have investigated two regression-based downscaling methodologies in the context of a linear regression transfer function of the form (1), using reanalysis data at large scales (NCEP-2 predictors) and station measurements of surface wind speed at small scales in the calibration. This approach might be expected to yield reasonably robust regression relations, since it is comprised largely of observations. However, our findings show that often this is not the

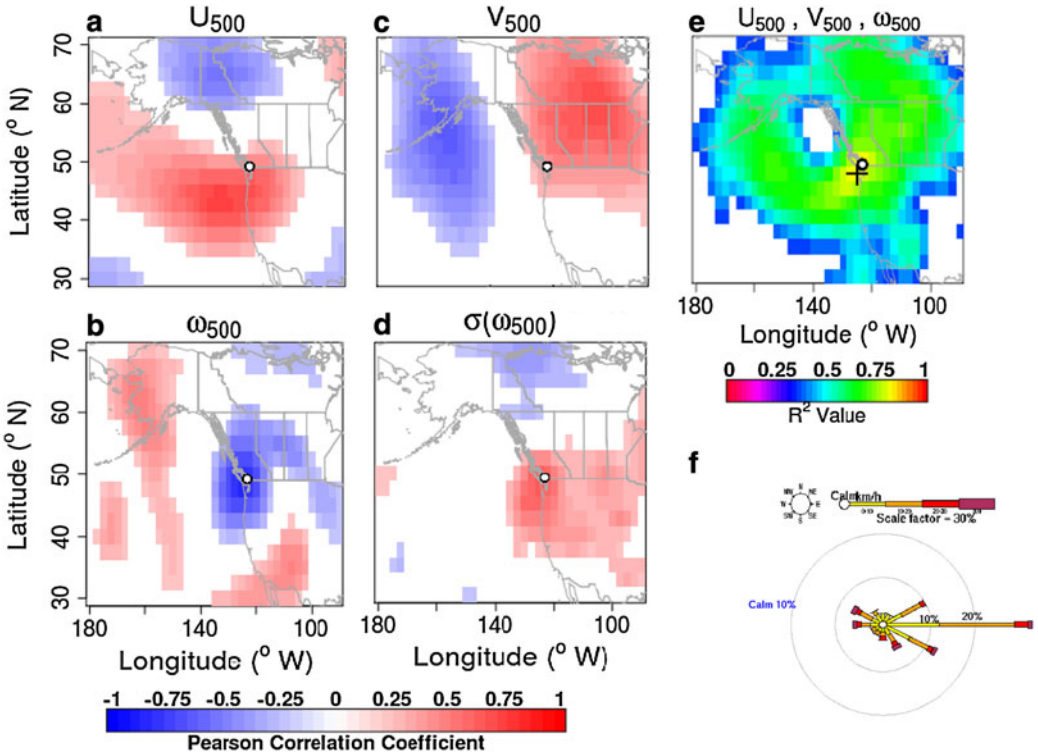

Fig. 12 Spatial distribution of correlation r for single-predictor regressions at Vancouver (open circle) in DJF (a–d), and R^2 for multiple regression using the three wind components as predictors (e), with the Weibull A parameter as predictand. The blue cross in panel e shows the grid cell with the largest R^2 value (= 0.82 in this case). The surface (hourly) wind rose for this station in DJF is shown in f. Concentric circles behind the wind rose indicate the frequency of observed winds that originate from various directions, while the size of the central circle reflects the proportion of calm winds relative to the total number of observations

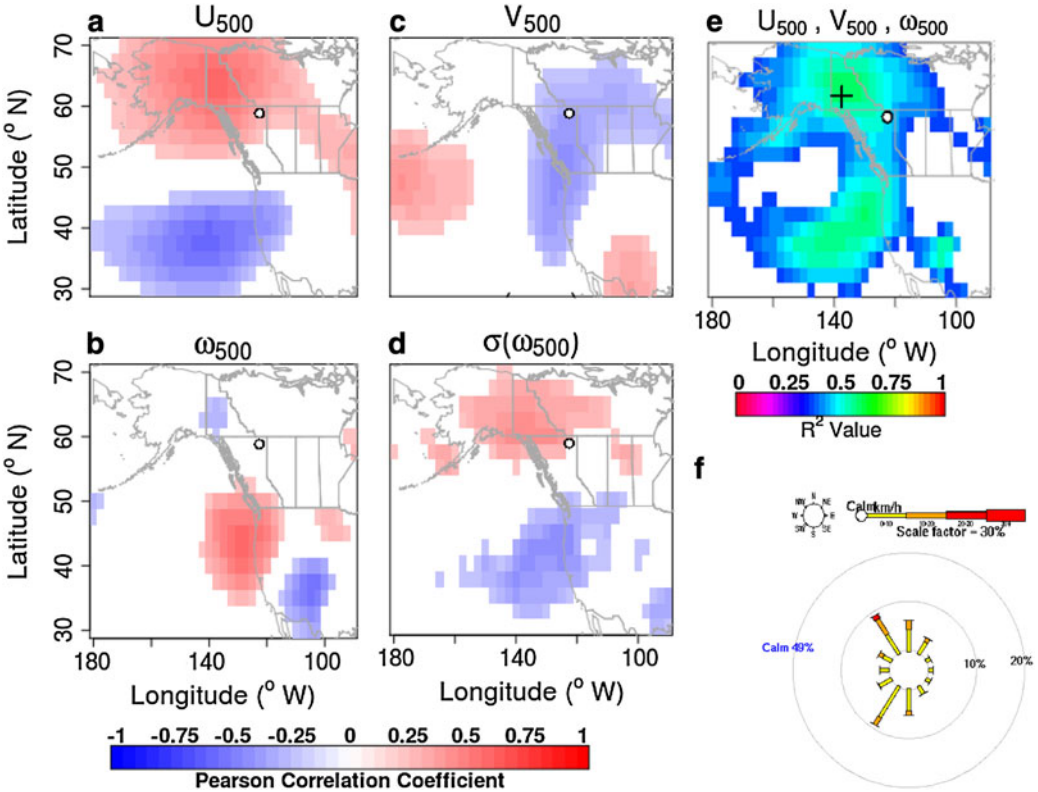

Fig. 13 Same as Fig. 12 but for Fort Nelson. The maximum R^2 value in panel e = 0.59 in this case

case. When the predictand and predictors are climatological monthly means, an important drawback was clearly identified: the variation in both is dominated by the region-wide annual cycle, leaving little local signal due to climate behavior at individual stations. Moving to an interannual technique obviates this concern, but displays only modest predictive power in fall and winter and considerably less skill in spring and summer. The examination of large-scale correlation patterns for individual stations suggests that a significant portion of the observed variance in monthly mean wind speed arises from predictor behaviour at some distance from the stations. This suggests that downscaling skill is limited by using predictor information from the nearest large-scale grid point only.

The results of the techniques employed in this paper suggest several possible research directions in the ongoing effort to produce improved downscaled wind results in BC and other regions of complex topography. The basic assumption of this work at the outset was that the monthly variance of surface wind speed at the local scale is associated with the corresponding monthly variance in the chosen predictor fields at a much larger scale. The limited success of the techniques examined under this assumption suggests a reexamination of the following: (1) the time sampling employed in the analysis; (2) the characteristic height of the predictors; and (3) the choice of predictors. Regarding the first point, it is known that strong variations in surface winds occur on the sub-daily timescale in the analysis region, especially in summer. The principal causes of these variations are mesoscale thermal circulations (e.g., land/sea breeze near the coast, along-slope flows in regions with steep topography; Whiteman 2000). While most of this variability occurs at spatial scales smaller than that of the NCEP-2 reanalysis, local mesoscale circulations are influenced by large-scale pressure gradients and temperature distributions, and these may carry information pertinent to small-scale surface wind behaviour. Nevertheless, the poor predictive ability found here for surface wind in summer, when diurnal effects are strongest, may be attributable to the chosen averaging time scale. The degradation of a similar regression-based approach for surface temperature in coastal Oregon (due south of BC) in summer was noted by Wigley et al. (1990).

Second, there is the issue of the relation between 500 hPa predictors and the same fields and wind speed at the surface. It is a common strategy to use fields at 500 hPa in order to avoid topography. However, the interaction of topography with the large-scale flow closer to the surface can exert a strong influence on the behaviour of surface wind (as e.g., at Vancouver, as discussed in Sect. 4). A consequence of this is reduced predictive power for the regression relations constructed using 500 hPa predictors alone, if the fields are sufficiently baroclinic that lower tropospheric fluctuations are not simply related to those in the mid-troposphere. Although fields closer to the surface tend to be "noisier" than those aloft, this may be a necessary evil when it comes to deriving effective downscaling relations.

Regarding the third issue, there are valid reasons for questioning the fundamental connection between W and the various large-scale atmospheric fields used as predictors in the current study—is such a link expected from atmospheric dynamics? In their recent study of a topographically complex region in southern France, Salameh et al. (2009) used roughly the same predictors but did not use W as a predictand, instead predicting the zonal and meridional surface wind components separately. With their regression-based downscaling, these authors were generally able to explain a higher fraction of the variance in wind components than we were able to explain in total wind speed in this work (although since many more predictor fields were used, the R^2 values were possibly inflated by overfitting). The only exceptions occurred when a particular component coincided with the cross-valley direction in a narrow valley, in which case the authors comment that "the unexplained variance is due to small scale turbulence or to [a] very localized source of perturbation."

In Paper II (van der Kamp et al. 2011; see also the recent work of Monahan 2011 on downscaling of sea surface winds), we examine differences between predictability of surface wind speeds and vector winds (i.e., including directional information) over the same region studied here, and further consider the reasons for significant differences in the explained variance using both methods. There it is shown that there are limits to the predictability of surface winds using predictors of the type considered in the present paper. By contrast, the use of vector wind components as predictands is not subject to such limitations to the same degree, and may offer a promising path to obtaining more reliable downscaling results.

Acknowledgments This work was supported by a Knowledge Synthesis Grant from the Canadian Foundation for Climate and Atmospheric Sciences. The authors would like to thank Gerd Buerger, Greg Flato, Yanping He, and two anonymous referees for comments on the manuscript and Dave Rodenhuis for his encouragement and interest in this work.

Appendix

Beginning with the simplest case of univariate linear regression of a monthly mean predictor variable P against a predictand y, the correlation coefficient is

$$r^2 = \frac{\mathrm{cov}^2(P,y)}{\sigma_{P_j}^2 \sigma_y^2}, \quad \mathrm{cov}(P,y) = M^{-1} \sum_{m=1}^{M_k} y_m P_m,$$
$$\sigma_y^2 = M^{-1} \sum_{m=1}^{M_k} y_m^2, \quad \sigma_P^2 = M^{-1} \sum_{m=1}^{M_k} P_m^2$$

where cov(P, y) is the covariance of P and y over the $M = 12$ month period of interest and the σ's are the

corresponding variances. The above assumes that both predictor and predictand are expressed as monthly anomalies from their respective annual means, i.e., $\bar{y} = \bar{P} = 0$. For an exactly sinusoidal predictand with amplitude α and zero phase and a predictor with amplitude β and phase θ, we have

$$y_m = \alpha \sin \gamma_m, \quad P_m = \beta \sin(\gamma_m + \theta),$$

where $\gamma_m = 2\pi m/12$. Evaluating r^2, one finds that the amplitudes in the quotient cancel, leaving:

$$r^2 = \cos^2\theta.$$

That is, r^2 differs from unity only inasmuch as the predictor-predictand phase difference differs from zero.

For two or more predictors P_j, with $P_j = \beta_j \sin(\gamma_m + \theta_j)$, the coefficient of determination is given by the appropriate generalization of the above, i.e.,

$$R^2 = \sum_{j=1}^{N} b_j \frac{\mathrm{cov}(P_j, y)}{\sigma_y^2}, \quad \mathrm{cov}(P_j, y) = M^{-1} \sum_{m=1}^{M_k} y_m P_{j,m},$$

where b_j are the coefficients of the best-fit multilinear function to the predictand y, determined by minimization of the least squares error:

$$\chi^2 = \sum_{m=1}^{M} \left[y_m - \left(a + \sum_{m=1}^{N} b_j P_{j,m} \right) \right]^2.$$

The resulting matrix equation,

$$\mathbf{Y} = \mathbf{A} \cdot \mathbf{B},$$

$$\mathbf{Y} = \begin{pmatrix} \sum_m y_m \\ \sum_m P_{1m} y_m \\ \sum_m P_{2m} y_m \\ \vdots \\ \sum_m P_{Nm} y_m \end{pmatrix}, \quad \mathbf{B} = \begin{pmatrix} a \\ b_1 \\ b_2 \\ \vdots \\ b_N \end{pmatrix},$$

$$\mathbf{A} = \begin{pmatrix} M & \sum_m P_{1m} & \sum_m P_{2m} & \cdots & \sum_m P_{Nm} \\ \sum_m P_{1m} & \sum_m P_{1m}^2 & \sum_m P_{1m} P_{2m} & \cdots & \sum_m P_{1m} P_{Nm} \\ \sum_m P_{2m} & \sum_m P_{2m} P_{1m} & \sum_m P_{2m}^2 & \cdots & \vdots \\ \vdots & \vdots & \vdots & \ddots & \vdots \\ \sum_m P_{Nm} & \sum_m P_{Nm} P_{1m} & \cdots & \cdots & \sum_m P_{Nm}^2 \end{pmatrix},$$

may be solved for the b_j as

$$b_j = \frac{|\mathbf{A}'(j+1)|}{|\mathbf{A}|},$$

where $\mathbf{A}'(j)$ is equal to $\mathbf{A}$ with the jth column replaced by $\mathbf{y}$.

As will become clear, performing the calculation for $N = 2$ is sufficient to establish a general result that holds for any number of predictors. After some straightforward algebra and noting that sums of odd periodic functions (e.g., $\sin[\gamma_i + \theta]$, etc.) over a complete period vanish, one finds:

$$b_1 = \frac{|\mathbf{A}'(2)|}{|\mathbf{A}|} = \frac{\alpha}{\beta_1} \frac{\cos\theta_1 - \cos\theta_2 \cos(\theta_1 - \theta_2)}{\sin^2(\theta_1 - \theta_2)}$$

$$b_2 = \frac{|\mathbf{A}'(3)|}{|\mathbf{A}|} = \frac{\alpha}{\beta_2} \frac{\cos\theta_2 - \cos\theta_1 \cos(\theta_1 - \theta_2)}{\sin^2(\theta_1 - \theta_2)}$$

$$\sigma_y^2 = 6\alpha^2 M^{-1}, \quad \mathrm{cov}(P_1, y) = 6\alpha\beta_1 M^{-1} \cos\theta_1,$$
$$\mathrm{cov}(P_2, y) = 6\alpha\beta_2 M^{-1} \cos\theta_2 .$$

Finally, constructing R^2, the amplitudes again cancel, leaving

$$R^2 = \frac{\cos^2\theta_1 + \cos^2\theta_2 - 2\cos\theta_1 \cos\theta_2 \cos(\theta_1 - \theta_2)}{\sin^2(\theta_1 - \theta_2)} = 1,$$

where the latter follows by using trigometric identities. This establishes the general result that only two sinusoidal predictors are needed to give perfect correlation with a sinusoidal predictand. It mirrors the well known result that any sinusoidal function with a given frequency and phase can be expressed as a linear combination of sines and cosines of the same frequency but zero phase, provided that certain definite relations hold between the various coefficients and phases (Davis 1963). While such an exact relation cannot obtain here due to the independence of predictand/predictor amplitudes and phases, it is still the case that complete correlation is obtained on the basis of the additional degrees of freedom provided by multiple predictors.

References

Abeysirigunawardena DS, Gilleland E, Bronaugh D, Wong P (2009) Extreme wind regime responses to climate variability and change in the inner south coast of British Columbia, Canada. Atmos-Ocean 47:41–61

Barry RG, Chorley RJ (1977) Atmosphere, weather, and climate, 3rd edn. Methuen, London, p 148

Burnham KP, Anderson DR (2002) Model selection and multimodel inference: a practical information-theoretic approach, 2nd edn. Springer, New York

Chang EKM, Lee S, Swanson KL (2002) Storm track dynamics. J Climate 15:2163–2183

Conradsen KL, Nielsen B, Prahm LP (1984) Review of Weibull statistics for estimation of wind speed distributions. J Appl Meteorol Clim 23:1173–1183

Davis HF (1963) Fourier series and orthogonal functions. New York, Dover

de Rooy WC, Kok K (2004) A combined physical—statistical approach for the downscaling of model wind speeds. Weather Forecast 19:485–495

Giorgi F, Hewitson B, Christensen J, Hulme M, Von Storch H, Whetton P, Jones R, Mearns L, Fu C (2001) Regional climate information—evaluation and projections. In: Houghton JT, Ding Y, Griggs DJ, Noguer M, van der Linden PJ, Xiaosu D (eds) Climate change 2001: the scientific basis. Cambridge University Press, Cambridge, pp. 583–638

Hanawa K, Ishizaki S, Tanimoto Y (1996) Examination of the strengthening of wintertime mid-latitude westerlies over the North Pacific in the 1970s. J Meteorol Soc Jpn 74:715–721

He Y, Monahan AH, Jones CG, Dai A, Biner S, Caya D, Winger K (2010) Probability distributions of land surface wind speeds over North America. JGR Atmospheres. doi:10.1029/2008JD010708

Justus CG, Hargraves WR, Mikhail A, Graber D (1978) Methods for estimating wind speed frequency distributions. J Appl Meteorol 17:350–353

Kanamitsu M, Ebisuzaki W, Woollen J, Yang S-K, Hnilo JJ, Fiorino M, Potter GL (2002) NCEP/DOE AMIP-II reanalysis (R-2). Bull Am Meteorol Soc 83:1631–1643

Lange, OS (2003) Living with weather along the British Columbia coast: the veil of chaos. Environment Canada/National Library of Canada, Vancouver

Marengo JA et al (2010) Future change of climate in South America in the late twenty-first century: intercomparison of scenarios from three regional climate models. Clim Dyn 35:1073–1097

Mass C (2008) The weather of the Pacific Northwest. University of Washington Press, Seattle

Merryfield WJ, Pal B, Foreman MGG (2009) Projected changes in surface marine winds off the west coast of Canada. JGR Atmospheres. doi:10.1029/2008JC005123

Michelangeli P-A, Vrac M, Loukos H (2009) Probabilistic downscaling approaches: application to wind cumulative distribution functions. Geophys Res Lett. doi:10.1029/2009GL038401

Monahan AH (2006) The probability distribution of sea surface winds. Part I: Theory and SeaWinds observations. J Climate 19:497–520

Monahan AH (2011) Can we see the wind? Statistical downscaling of historical sea surface winds in the northeast subarctic Pacific. J Clim (submitted)

Music B, Caya D (2007) Evaluation of the hydrological cycle over the Mississippi River Basin as simulated by the Canadian regional climate model (CRCM). J Hydrometeor 8:969–988

Pryor SC, Schoof JT, Barthelmie RJ (2005) Empirical downscaling of wind speed probability distributions. JGR Atmospheres 110:D19109

Pryor SC, Schoof JT, Barthelmie RJ (2006) Winds of change? Projections of near-surface winds under climate change scenarios. Geophys Res Lett 33. doi:10.1029/2006GL026000

Sailor DJ, Li X (1999) A semiempirical downscaling approach for predicting regional temperature impacts associated with climatic change. J Clim 12:103–114

Sailor DJ, Hu T, Li X, Rosen JN (2000) A neural network approach to local downscaling of GCM output for assessing wind power implications of climate change. Renew Energy 19:359–378

Sailor DJ, Smith M, Hart M (2008) Climate change implications for wind power resources in the Northwest United States. Renew Energy 33:2393–2406

Salameh T, Drobinski P, Vrac M, Naveau P (2009) Statistical downscaling of near-surface wind over complex terrain in southern France. Meteorol Atmos Phys 103:253–265. doi:10.1007/s00703-008-0330-7

Sloughter JM, Gneiting T, Raftery AE (2010) Probabilistic wind speed forecasting using ensembles and Bayesian model averaging. J Am Statist Assoc 105:25–35

Stewart DA, Essenwanger OM (1978) Frequency distribution of wind speed near the surface. J Appl Meteorol 17:1633–1642

Thorarinsdottir TL, Gneiting T (2010) Probabilistic forecasts of wind speed: ensemble model output statistics by using heteroscedastic censored regression. J R Statist Soc A 173:371–388

Troen I, Petersen EL (1989) European wind atlas. Riso National Laboratory, Roskilde

Tuller SE (2004) Measured wind speed trends on the west coast of Canada. Int J Climatol 24:1359–1374

Tuller SE, Brett AC (1985) The goodness of fit of the Weibull and Rayleigh distributions of observed winds in a topographically diverse area. J Climatol 5:79–94

Van der Auwera L, de Meyer F, Malet LM (1980) The use of the Weibull three-parameter model for estimating mean wind power densities. J Appl Meteorol 19:819–825

van der Kamp D, Curry CL, Monahan AH (2011) Statistical downscaling of historical monthly mean winds over a coastal region of complex terrain. II. Predicting wind components. Clim Dyn. doi:10.1007/s00382-011-1175-1

Wan H, Wang XL, Swail VR (2010) Homogenization and trend analysis of Canadian near-surface wind speeds. J Climate 23:1209–1225. doi:10.1175/2009JCLI3200.1

Wang S-Y, Gillies RR, Takle ES, Gutowski WJ Jr (2009) Evaluation of precipitation in the intermountain region as simulated by the NARCCAP regional climate models. Geophys Res Lett 36:L11704. doi:10.1029/2009GL037930

Whiteman CD (2000) Mountain meteorology: fundamentals and applications. Oxford University Press, New York

Wigley TML, Jones PD, Briffa KR, Smith G (1990) Obtaining subgrid-scale information from coarse-resolution general circulation model output. J Geophys Res 95:1943–1953

Wilby RL, Wigley TML, Conway D, Jones PD, Hewitson BC, Main J, Wilks DS (1998) Statistical downscaling of general circulation model output: a comparison of methods. Water Resour Res 34:2995–3008

Wilks DS (1995) Statistical methods in the atmospheric sciences: an introduction. Academic Press, San Diego